

Optical field control via liquid crystal photoalignment

Wei Ji, Bing-Yan Wei, Peng Chen, Wei Hu & Yan-Qing Lu

To cite this article: Wei Ji, Bing-Yan Wei, Peng Chen, Wei Hu & Yan-Qing Lu (2017) Optical field control via liquid crystal photoalignment, *Molecular Crystals and Liquid Crystals*, 644:1, 3-11, DOI: [10.1080/15421406.2016.1277314](https://doi.org/10.1080/15421406.2016.1277314)

To link to this article: <http://dx.doi.org/10.1080/15421406.2016.1277314>



Published online: 27 Apr 2017.



Submit your article to this journal [↗](#)



Article views: 8



View related articles [↗](#)



View Crossmark data [↗](#)

Optical field control via liquid crystal photoalignment

Wei Ji, Bing-yan Wei, Peng Chen, Wei Hu, and Yan-qing Lu

National Laboratory of Solid State Microstructures, College of Engineering and Applied Sciences, and Collaborative Innovation Center of Advanced Microstructures, Nanjing University, Nanjing, China

ABSTRACT

Optical field control of laser beams is realized through photo-aligned liquid crystals. A dynamic micro-lithography system combined with a polarization-sensitive alignment agent is utilized to perform arbitrary fine liquid crystal alignment. Fork gratings are fabricated to generate high quality optical vortices. Forked polarization gratings with space-variant liquid crystal azimuthal orientations are proposed and corresponding optical vortices with arbitrary azimuthal and radial indices are demonstrated in high efficiency. Moreover, Airy masks for polarization selective Airy beam generation and polarization converters suitable for arbitrary vector beams are fabricated. This technology drastically enhances the capability of optical field control.

KEYWORDS



Liquid crystals; photoalignment; fork gratings; optical field control

1. Introduction

Optical field control has attracted growing interests over the past few years, which is driven by the ever-increasing demand for its use in lithography, optical trapping and other applications [1]. The typical cases of specific optical fields include vortex beams [2], Airy beams [3] and vector beams [4]. Over the past decades, a device called spatial light modulator (SLM) has been widely used. Although it allows on-demand selection of arbitrary laser modes in real-time with a wide dynamic range of phase values [5], it suffers from several shortcomings such as optical inefficiency, the size mismatch with the incident beam and limited beam quality. Hence, exploring new high efficient approaches for beam steering is in urgent demand.

Liquid crystals (LCs), exhibiting broadband birefringence and excellent electrical tunability [6], have been widely used to control optical field since most parameters of light such as intensity, phase, polarization and even wavefront could be instantly controlled. Typically, patterned electrodes [7–9], micro-rubbing [10], photoalignment [11–14] and polarization holography [15] are usually used to realize patterned LCs. Among them, photoalignment has been proved to be a suitable approach for the creation of high quality multi-domain LC alignment with resolution up to 1 μm . Therefore, azimuthal angle control for micro-patterned LC could be conveniently accomplished.

To make full use of the advantages of photoalignment, a digital micro-mirror device (DMD) based micro-lithography system was developed to accomplish arbitrary and accurate alignment patterns dynamically. By introducing a motorized rotating polarizer, not only the high-quality LC binary fork gratings for the generation of arbitrary optical vortices (OVs),

CONTACT Wei Hu  huwei@nju.edu.cn  National Laboratory of Solid State Microstructures, College of Engineering and Applied Sciences, and Collaborative Innovation Center of Advanced Microstructures, Nanjing University, Nanjing 210093, China. Color versions of one or more of the figures in the article can be found online at www.tandfonline.com/gmcl.

© 2017 Taylor & Francis Group, LLC

but also the forked polarization gratings (FPGs) with continuously space-variant director distributions were fabricated. Especially, FPGs can generate OV in high conversion efficiency and exhibit polarization controllability, and OVs with arbitrary azimuthal and radial indices could be easily generated. What's more, polarization Airy masks for Airy beam generation, and polarization converters for generating arbitrary vector beams were also demonstrated. The proposed technique supplies a universal and practical approach for optical field control.

2. A dynamic micro-lithography system based photo-patterning

A sulphonic azo-dye SD1 was used as the photoalignment agent [16]. When illuminated by linearly polarized UV light, the azo dye molecules tend to reorient their absorption oscillators perpendicular to the incident polarization. Furthermore, SD1 is rewritable and only the last photo-reorientation will be recorded. Glass substrates of the LC cell were spin coated with 0.5% solution of SD1 in dimethylformamide (DMF) for 40 s at 3000 rpm and then after the evaporation of the solvent by soft-baking at 100°C for 5 min. Afterwards, two substrates were assembled together by using dielectric spacers to define the cell gap.

A DMD based micro-lithography system [12] was applied to transfer the designed patterns into the SD1 layers, as shown in Fig. 1. A UV lamp with a filter of 320–390 nm was used as the collimated light source. Then the light beam was reflected onto the DMD (Discovery 3000, Texas Instruments) controlled by the computer and carried on a designed pattern. After being focused by an objective lens and polarized by a polarizer attached to rotating mounts through step-motors, the beam then projected onto the LC cell or one glass substrate coated with alignment layers. Moreover, a charge coupled device (CCD) was utilized to monitor the focusing process. Thanks to the polarization-sensitivity and rewritability of SD1 molecules, the photo-patterning procedure was drastically facilitated. Arbitrary alignment direction control can also be realized by rotating the polarizer while changing the pattern. After LC E7 was capillary filled, the orientation of SD1 would be transferred to LC by intermolecular interactions. Owing to the excellent flexibility of image output capability of DMD, arbitrary fine photo-patterned LCs can be conveniently obtained.

3. LC forked gratings for generating vortex beams

Among all the specific optical fields, OVs are particularly attractive and have been widely used in optical tweezers, quantum data encryption and so on. OVs are characterized by helical phase fronts and donut-shaped intensity distributions. The specific phase distribution results in an orbital angular momentum (OAM), adding another degree of freedom in the manipulation of light, wherein m represents the topological charge. Till now, several means have been proposed for OV generation [2], like direct rephrasing of a plane wave via spiral phase plates, mode conversion via an astigmatic system, a novel LC element “q-plate” and other pioneering methods based on meta-surfaces. Apart from the above setups and elements, another alternative choice is diffraction gratings with dislocations centered at the beam axis called “fork” gratings. Here gives an example of a fork grating with $m = 1$ as shown in Fig. 2(a). Since the fork grating is a computer-generated hologram of the plane wave and an optical vortex, it carries information of the topological charge m and the reference wave. When a Gaussian beam illuminates the fork grating, the beam is then reconstructed and a series of helically phased beams are produced in the diffraction orders.

Via the home-made DMD based photo-patterning technology, several LC fork gratings were demonstrated [17]. Figure 2(b) exhibits the micrograph of the LC fork grating with $m = 1$

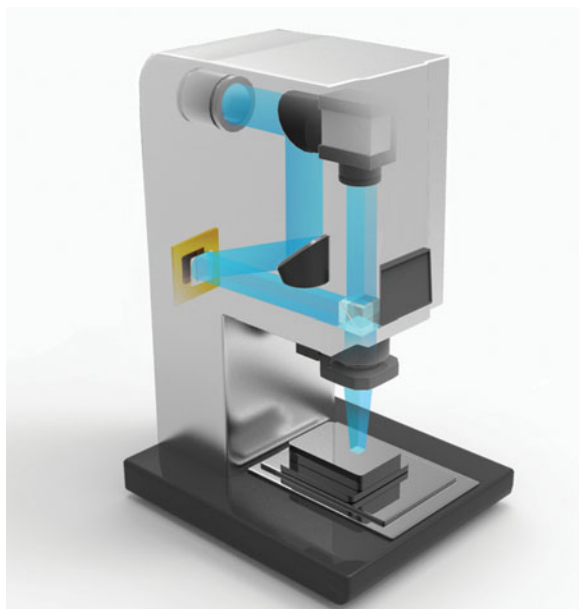


Figure 1. Schematic illustration of the DMD based micro-lithography system. It consists of a light emission part, a dynamic pattern generation part, an image focusing part and a monitor part.

of alternative twisted nematic (TN) and planar aligned (PA) domains under a cross-polarized microscope with the polarizer fixed parallel to the LC director at the input end. Herein, the hologram with designed topological charge was recorded on a homogeneously pre-aligned substrate by a two-step photo-exposure process, and then the substrate was assembled with another homogeneously aligned one to form the cell [18]. The micrograph with the TN region in bright state and the PA region in dark state reveals a faithful replica of the computer-generated hologram as shown in Fig. 2(a). To further characterize the fabricated fork grating, the corresponding diffraction pattern is captured as shown in Fig. 2(e). As expected, a series of OV's are produced in the diffraction orders on both sides of the 0th order, and the topological charge increases as the diffraction order increasing. In spite of a slight beam extension in higher orders, the diffraction pattern indicates the high quality of the obtained LC fork grating. However, the conversion efficiency for TN/PA configuration is quite limited [19] and polarization dependent, which limits its applications.

In order to address above issue, two fork gratings in specific alignment modes are fabricated. Figure 2(c) shows a fork grating consisting of two complementary hybrid aligned nematic (HAN) domains. In this cell, one substrate is coated with SD1 layer recorded orthogonally homogeneous fork grating pattern, and the other is coated with a polyimide layer uniformly rubbed at 45° with respect to the PA orientation to perform vertical alignment. Moreover, a LC fork grating with an orthogonal PA pattern [20] is presented in Fig. 2(d). The uniformity in Figs. 2(c) and (d) proves the high quality and excellent orthogonality of the alignment and demonstrates the accuracy of the technology.

Several tests were carried out on the orthogonal HAN sample. A 671 nm laser beam illuminated the sample with its diffraction patterns captured by a detector or a CCD, and curves of voltage-dependent efficiency (i.e., V - η curves) of the 1st order were also plotted in Fig. 3. Here, the efficiency is defined as the intensity ratio of the 1st diffraction order to the total incident light. While rotating the sample, the curves are quite similar. As shown in Fig. 3, V - η curves of different incident polarization (0° , 45° and 90°) are exhibited, demonstrating the excellent

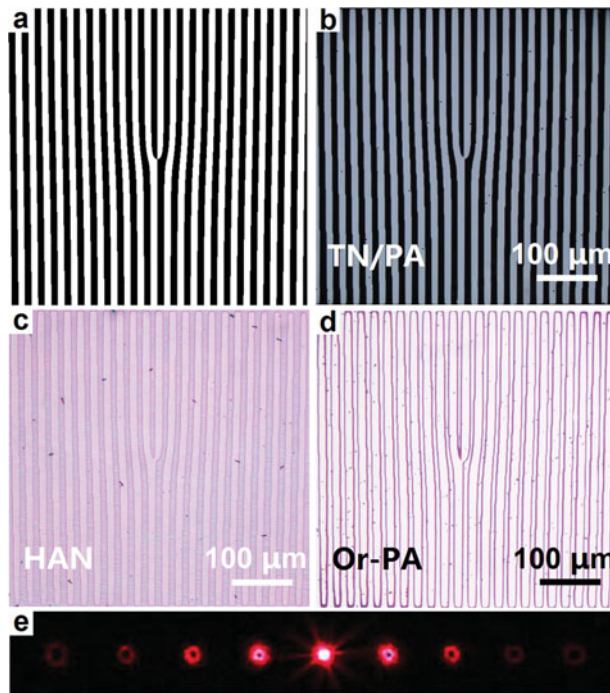


Figure 2. (a) The computer-generated hologram of $m = 1$. Micrographs of (b) a TN/PA, (c) an orthogonal HAN and (d) an orthogonal PA fork grating with $m = 1$. (e) The diffraction orders of a TN/PA fork grating.

polarization independency. This is because the two perpendicular components derived from all incident light experience a same refractive index change. When $1.7 V_{\text{rms}}$ is applied, the efficiency η reaches a maximum of 37%, that is 74% for total $\pm 1\text{st}$ orders, showing the “on” state of OV. In addition, the corresponding diffraction pattern is shown as inset. This is because under this condition, the phase retardation between the o-ray and e-ray is π . When the voltage is increased to $10 V_{\text{rms}}$, the phase retardation is reduced to nearly zero, thereby the $\pm 1\text{st}$

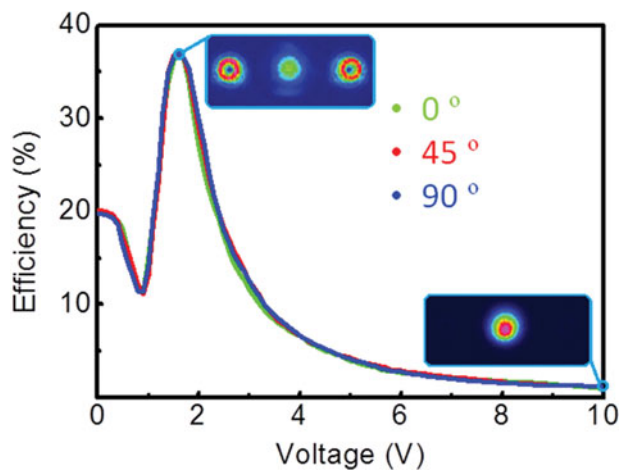


Figure 3. V - η curves of the 1st order optical vortex of an or-HAN LC fork grating with $m = 1$ at different incident polarization angles: 0° , 45° and 90° . Insets are the diffraction patterns captured at the voltage of $1.7 V_{\text{rms}}$ and $10 V_{\text{rms}}$.

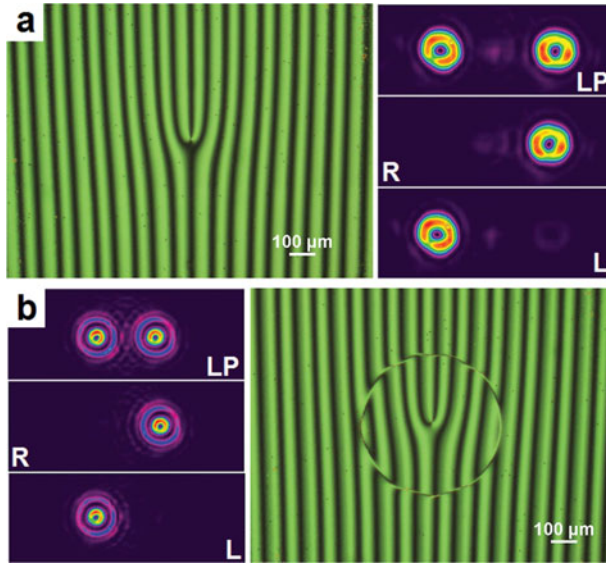


Figure 4. Micrographs and diffraction patterns of FPG samples with (a) $m = 1, p = 0$ and (b) $m = 1, p = 1$. The polarization of the incident beams are labelled in the image. LP: linearly polarized light. R: right circularly polarized light. L: left circularly polarized light.

orders are highly suppressed, leaving only a standard Gaussian beam in the center as shown in the inset, which is defined as the “off” state. Thus, dynamic switching between Gaussian modes and vortex beams can be achieved through changing the applied voltages.

Thanks to the good electro-optical tunability of LCs, equivalent high efficiencies could be achieved for different wavelengths by tuning the applied voltages, which eliminates the cost of preparing different elements for different wavelengths. Moreover, since SD1 is optical rewritable, the hologram pattern could be erased by a uniform linearly polarized light and then rewritten by the dynamic micro-lithography system to obtain a new hologram with different m . The above two merits endow LC fork gratings with great potentials for a wide range of applications.

4. LC forked polarization gratings

To further improve the conversion efficiency, we introduce the Pancharatnam-Berry (PB) phase into the fork grating and propose LC forked polarization gratings (FPGs) [21], which owns the space-variant director distributions. For such optical devices, the input energy can be totally diffracted into a single order [22]. While a Gaussian beam illuminates the FPG, only three diffraction orders exist: the 0th order, a Gaussian mode with the same polarization as the input one, and the ± 1 st orders, which are always circularly polarized and orthogonal to each other with OAM of opposite m . The intensity distribution between the 0th and the ± 1 st orders depends on the phase retardation and the incident polarization. If the phase retardation equals π (half-wave condition), only the ± 1 st orders exist, and if the input light is circularly polarized, only one OV with orthogonal circular polarization will be obtained.

For such FPGs, the LCs exhibit space-variant azimuthal orientations, which is different from the binary fork gratings. To realize the unique design, a multi-step partly overlapping exposure is carried out [21]. Figure 4(a) shows the micrograph of a FPG with $m = 1$ under a polarized optical microscope. The continuous change of the brightness results from the

continuous varying of the LC directors, with the dark domains corresponding to the regions of LC directors approximately parallel and the bright domains corresponding to regions of directors around 45° to the polarizer or the analyzer. When rotating the sample, the dark and bright domains interconvert gradually, confirming the continuous varying of the director of the FPG. The diffraction patterns with different incident polarization are also captured. Here, a suitable voltage is applied to get a half-wave condition. When linearly polarized Gaussian beam incidents the FPG, a maximum $\eta_{\pm 1} \approx 98.5\%$ is achieved, and both the first orders can be clearly observed as shown in the right-top image in Fig. 4(a). When illuminated by a left/right circularly polarized beam, only the $+1\text{st} / -1\text{st}$ order exists as shown in the right-middle and bottom images in Fig. 4(a), indicating a strong polarization control effect. That means the dynamic energy distribution between the $\pm 1\text{st}$ orders could be accomplished by changing the incident polarization.

Laguerre-Gaussian (LG) modes give a more general description of OV's and there are two featured indices: m , the topological charge, and p , the radial indices. For above case, $p = 0$, which exhibits a donut-like intensity distribution. If p is a positive integer, the mode will present $p + 1$ concentric rings. Here, a more complex FPG ($m = 1, p = 1$) is demonstrated in Fig. 4(b). There is a circular disclination observed because of the $\pi/2$ shift of the LC director astride the discontinuities. When illuminated with a Gaussian beam, the diffracted OV's present two bright rings. The performance of this FPG is similar to the simple one, and the diffraction patterns captured at the maximum diffraction efficiency when illuminated with linearly, left, and right circularly polarized light are shown on the left of Fig. 4(b). Similarly, arbitrary OV can be efficiently generated including OV's with $p > 1$ or even fractional m .

5. The generation of Airy beams and vector beams

Airy beams exhibit the distinguishing features of non-diffraction, transverse acceleration and self-healing [3], which have great potentials in the fields of optical manipulations, micro-fabrications, biology science and so on. However, for traditional LC Airy masks, two branches of Airy beam appear simultaneously. Here, we fabricated a LC polarization Airy mask (PAM) [23] with cubically space-variant azimuthal orientations. Figure 5(a) gives the micrograph of the PAM. The brightness varies continuously, indicating the precise control of LC alignment. To characterize the performance of the PAM, a 671 nm laser propagates through the PAM with the phase retardation fixed at half-wave condition and a spherical lens, then the resultant Airy beam is captured by a CCD camera. When a linearly polarized Gaussian beam illuminates the PAM, dual Airy beams occur, as shown in the three-dimensional image in Fig. 5(b). When a circularly polarized light inputs, only single Airy beam with orthogonal circular polarization appears as shown in Fig. 5(c). When compared with the simulated results shown as the inset, the obtained Airy beam is perfectly consistent with the simulation. By this means, polarization-controllable switch between single and dual Airy beams with high quality can be realized, and it may pave a way towards widespread applications even in some unexplored fields.

We also propose and demonstrate LC polarization converters [24] suitable for arbitrary VB generations. The converters are special TN cells characterized by one uniformly aligned substrate and the counter one with space-variant alignment. By the DMD based photo-aligning technique, various polarization converters are fabricated. Figure 6 (a) and (b) show the micrographs of polarization converters for the generation of azimuthally/radially polarized light under a crossed-polarized microscope. In the observation, the polarization of incident light

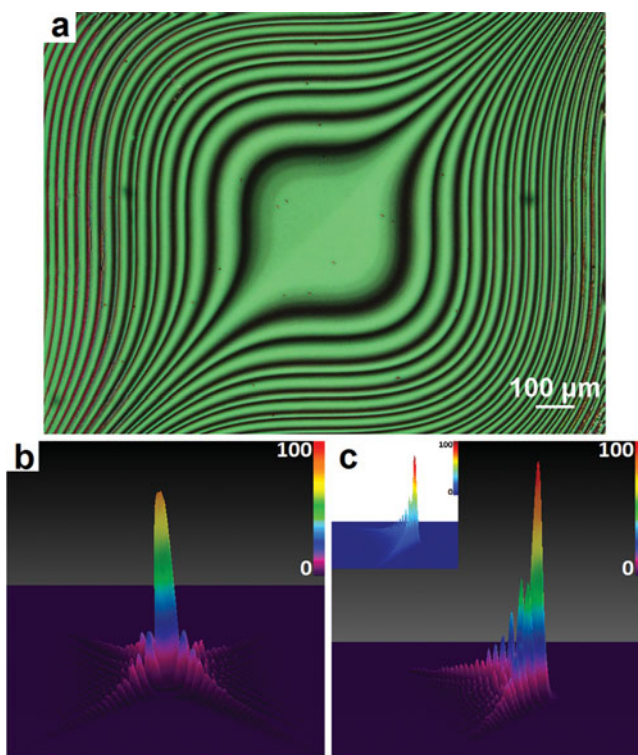


Figure 5. (a) The micrograph of a LC PAM. 3D intensity distributions of Airy beams illuminated by (b) linearly and (c) circularly polarized light with the inset showing the simulated result, respectively. The color bar indicates the relative optical intensity.

is parallel to the LC orientation at the uniformly aligned front substrate. In this case, the output polarization follows the local LC director distribution on the rear substrate, thus designed VBs (shown at the bottom left) are generated. More complicated polarization converters can also be fabricated to explore the capability of VB generation. One example of bi-ringed VB is shown in Fig. 6(c), which possesses a bi-ringed polarization distribution of radial and azimuthal polarization respectively. The obtained converters can be further utilized as polarization masks to implement vector-photoaligning. The technique facilitates both the volume duplication of these converters and the generation of another promising optical element, the q-plate [25], which is suitable for the generation of VBs for coherent lasers. Moreover, any kinds of LC devices mentioned in this work can also be fabricated by just one-step vector-photoaligning process using specially designed converters.

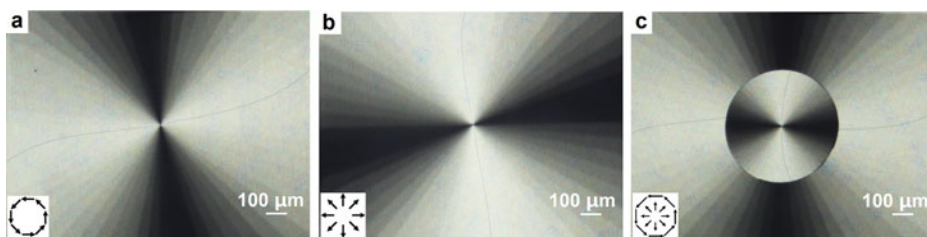


Figure 6. The experimental polarization distributions of VBs with (a) azimuthal, (b) radial polarization and (c) bi-ringed VB, with the schematic ones labelled at the bottom left.

6. Conclusion

In this work, arbitrary fine LC alignment control is realized by dynamic photo-aligning technique, thus several kinds of optical fields are generated with high quality. LC fork gratings and FPGs are fabricated for the arbitrary generation of OV. PAMs for Airy beam generation and polarization converters for generating arbitrary vector beams are demonstrated as well. The SD1 is compatible to the azimuthal angle control of LCs. For a given wavelength (visible, infrared to terahertz) [26–29], we can properly choose LC materials and precisely control the cell gap to optimize the conversion efficiency. As here absorptive electrodes can be avoided, the optical damage threshold could be drastically increased. In addition, thanks to the excellent electro-optical tunability of LCs, good tolerance to incident light wavelength and electrical switching between structured beams and Gaussian beams are achievable via tuning the applied voltage. Besides, these exhibit merits of compact size, low cost, simple configuration and easy fabrication. The proposed technology drastically enhances the capability of optical field control, and may bring more possibilities for the design of novel photonic devices.

Acknowledgements

The authors are indebted to Prof. V. Chigrinov for his kind support with photoalignment agent and technique. This work was supported by the [National Natural Science Foundation of China] under grants [number 11304151], [number 61490714], [number 61435008] and [number 61575093].

References

- [1] Woerdemann, M., Alpmann, C., Esseling, M., & Denz, C. (2013). *Laser Photonics Rev.*, 7, 839.
- [2] Yao, A. M., & Padgett, M. J. (2011). *Adv. Opt. Photonics*, 3, 161.
- [3] Siviloglou, G. A., Broky, J., Dogariu, A., & Christodoulides, D. N. (2007). *Phys. Rev. Lett.*, 99, 213901.
- [4] Zhan, Q. (2009). *Adv. Opt. Photonics*, 1, 1.
- [5] Ngcobo, S., Litvin, I., Burger, L., & Forbes, A. (2013). *Nature Commun.*, 4, 2289.
- [6] Yang, D. K., & Wu, S. T. (2006). *Fundamentals of Liquid Crystal Devices*, Wiley: England.
- [7] Liu, Y. J., Sun, X. W., Luo, D., & Raszewski, Z. (2008). *Appl. Phys. Lett.*, 92, 101114.
- [8] Ge, S. J., Ji, W., Cui, G. X., Wei, B. Y., Hu, W., & Lu, Y. Q. (2014). *Opt. Mater. Express*, 4, 2535.
- [9] Ge, S. J., Chen, P., Ma, L. L., Liu, Z., Zheng, Z. G., Shen, D., Hu, W., & Lu, Y. Q. (2016). *Opt. Mater. Express*, 6, 1087.
- [10] Honma, M., & Nose, T. (2012). *Appl. Phys. Lett.*, 101, 041107.
- [11] Schadt, M., Seiberle, H., & Schuster, A. (1996). *Nature*, 381, 212.
- [12] Wu, H., Hu, W., Hu, H. C., Lin, X. W., Zhu, G., Choi, J. W., Chigrinov, V., & Lu, Y. Q. (2012). *Opt. Express*, 20, 16684.
- [13] Ma, L. L., Li, S. S., Li, W. S., Ji, W., Luo, B., Zheng, Z. G., Cai, Z. P., Chigrinov, V., Lu, Y. Q., Hu, W., & Chen, L. J. (2015). *Adv. Opt. Mater.*, 3, 1691.
- [14] Chen, P., Ge, S. J., Ma, L. L., Hu, W., Chigrinov, V., & Lu, Y. Q. (2016). *Phys. Rev. Appl.*, 5, 044009.
- [15] Crawford, G. P., Eakin, J. N., Radcliffe, M. D., Callan-Jones, A., & Pelcovits, R. A. (2005). *J. Appl. Phys.*, 98, 123102.
- [16] Hegde, G., Kozenkov, V. M., Chigrinov, V. G., & Kwok, H. S. (2009). *Mol. Cryst. Liq. Cryst.*, 507, 41.
- [17] Wei, B. Y., Hu, W., Ming, Y., Xu, F., Rubin, S., Wang, J. G., Chigrinov, V., & Lu, Y. Q. (2014). *Adv. Mater.*, 26, 1590.
- [18] Hu, W., Srivastava, A., Xu, F., Sun, J. T., Lin, X. W., Cui, H. Q., Chigrinov, V., & Lu, Y. Q. (2012). *Opt. Express*, 20, 5384.
- [19] Li, J. N., Hu, X. K., Wei, B. Y., Wu, Z. J., Ge, S. J., Ji, W., Hu, W., & Lu, Y. Q. (2014). *Appl. Opt.*, 53, E14.
- [20] Hu, W., Srivastava, A., Lin, X. W., Liang, X., Sun, J. T., Zhu, G., Chigrinov, V., & Lu, Y. Q. (2012). *Appl. Phys. Lett.*, 100, 111116.

- [21] Chen, P., Wei, B. Y., Ji, W., Ge, S. J., Hu, W., Xu, F., Chigrinov, V., & Lu, Y. Q. (2015). *Photonics Res.*, 3, 133.
- [22] Duan, W., Chen, P., Wei, B. Y., Ge, S. J., Liang, X., Hu, W., & Lu, Y. Q. (2016). *Opt. Mater. Express*, 6, 597.
- [23] Wei, B. Y., Chen, P., Hu, W., Ji, W., Zheng, L. Y., Ge, S. J., Ming, Y., Chigrinov, V., & Lu, Y. Q. (2015). *Sci. Rep.*, 5, 17484.
- [24] Chen, P., Ji, W., Wei, B. Y., Hu, W., Chigrinov, V., & Lu, Y. Q. (2015). *Appl. Phys. Lett.*, 107, 241102.
- [25] Ji, W., Lee, C. H., Chen, P., Hu, W., Ming, Y., Zhang, L., Lin, T. H., Chigrinov, V., & Lu, Y. Q. (2016). *Sci. Rep.*, 6, 25528.
- [26] Wu, S. T. (1986). *Phys. Rev. A*, 33, 1270.
- [27] Wei, B. Y., Chen, P., Ge, S. J., Zhang, L. C., Hu, W., & Lu, Y. Q. (2016). *Photonics Res.*, 4, 70.
- [28] Ge, S. J., Liu, J. C., Chen, P., Hu, W., & Lu, Y. Q. (2015). *Chin. Opt. Lett.*, 13, 120401.
- [29] Wang, L., Lin, X. W., Hu, W., Shao, G. H., Chen, P., Liang, L. J., Jin, B. B., Wu, P. H., Qian, H., Lu, Y. N., Liang, X., Zheng, Z. G., & Lu, Y. Q. (2015). *Light Sci. Appl.*, 4, e253.